The Application of Plastic-Fracturing Theory to the Finite Element Analysis of General Reinforced Shells

Wilfried B. Krätzig, Wolfhard Zahlten
Institute for Statics and Dynamics, Ruhr-University, Bochum, FRG

1. INTRODUCTION

The paper presents a layered finite element model of high accuracy for thin reinforced concrete shells. Starting from a tensorial Kirchhoff-Love-type theory in curvilinear coordinates the discretized incremental functional of virtual work is established. Substitution of the plastic-fracturing model for concrete and elasto-plastic behavior with kinematic hardening for steel yields the physically nonlinear element matrices. Opening and closing of cracks is simulated by principal stress criteria. Finally, several computed responses are presented to demonstrate the efficiency of the derived numerical model.

2. THE NONLINEAR SHELL CONTINUUM

The reinforced concrete shell to be analyzed is modelled due to Fig. 1 as a multi-layered continuum. Each layer is related to a reference surface $\Theta^3 = 0$, usually the middle surface, on which increments of tensorial **stress resultants** and **stress couples** are defined as (Basar, Krätzig, 1985):

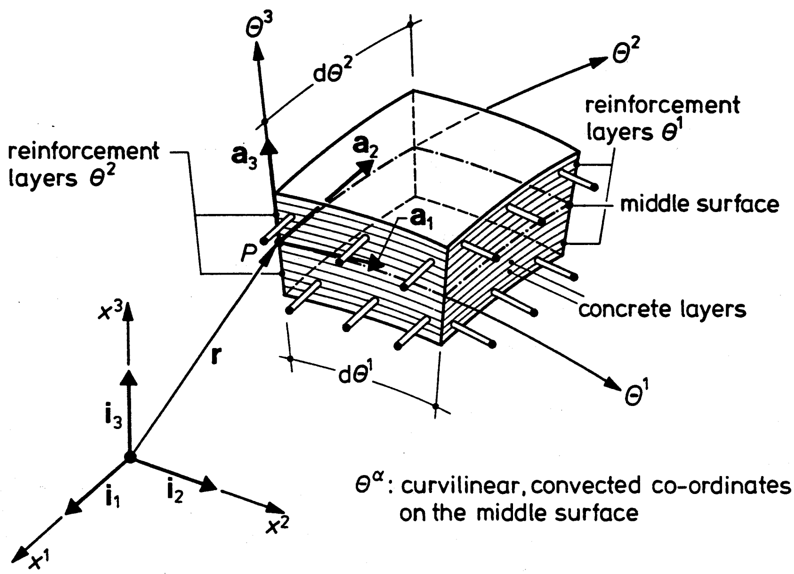

Fig. 1: Layered shell element

$$\Delta n^{\alpha\beta} = \int_h \mu\, \mu^\beta_\rho\, \tau^{\alpha\rho}\, d\Theta^3 , \qquad \Delta m^{\alpha\beta} = \int_h \mu\mu^\beta_\rho\, \tau^{\alpha\rho}\, \Theta^3\, d\Theta^3 \tag{2.1}$$

with: $$\mu^\beta_\rho = \delta^\beta_\rho - \Theta^3\, b^\beta_\rho , \quad \mu = |\mu^\beta_\rho| . \tag{2.2}$$

The individual layers are considered and described as membrane shells, fully bounded with their neighbors. Increments of the force variables (2.1) are related to increments of the 1. and 2. **strain tensors** $\Delta\alpha_{\lambda\mu}$, $\Delta\beta_{\lambda\mu}$ of the reference surface (Basar, Krätzig, 1985) by the general **constitutive relations**

$$\begin{aligned} \Delta n^{\alpha\beta} &= \overset{1}{C}{}^{\alpha\beta\lambda\mu}\, \Delta\alpha_{\lambda\mu} + \overset{2}{C}{}^{\alpha\beta\lambda\mu}\, \Delta\beta_{\lambda\mu} , \\ \Delta m^{\alpha\beta} &= \overset{2}{C}{}^{\alpha\beta\lambda\mu}\, \Delta\alpha_{\lambda\mu} + \overset{3}{C}{}^{\alpha\beta\lambda\mu}\, \Delta\beta_{\lambda\mu} , \end{aligned} \tag{2.3}$$

in which the coefficients

$$\overset{n}{C}{}^{\alpha\beta\lambda\mu} = \int_h \mu\, \mu^\beta_\rho\, C^{\alpha\rho\lambda\mu}\, (\Theta^3)^{n-1}\, d\Theta^3 \tag{2.4}$$

embody integral transforms of the tangential components of the nonlinear material tensor C^{ijkm} described in detail in the next chapter. $\Delta\alpha_{\lambda\mu}$, $\Delta\beta_{\lambda\mu}$ are connected to the displacement variables $u_i, w_\alpha, \overset{+}{u}_i, \overset{+}{w}_\alpha$ by nonlinear kinematic relations (Basar, 1986).

Equilibrium of a certain position of the shell, adjacent to a previous state of equilibrium, is finally guarantied by the incremental principle of virtual work $\delta A_i + \delta A_a = 0$ with

$$\begin{aligned} -\delta A_i &= \iint_F \{ n^{\alpha\beta}\, \delta\Delta\alpha_{\alpha\beta} + m^{\alpha\beta}\, \delta\Delta\beta_{\alpha\beta} + \overset{1}{C}{}^{\alpha\beta\lambda\mu}\, \Delta\alpha_{\lambda\mu}\, \delta\Delta\alpha_{\alpha\beta} \\ &\quad + \overset{2}{C}{}^{\alpha\beta\lambda\mu}\, (\Delta\beta_{\lambda\mu}\, \delta\Delta\alpha_{\alpha\beta} + \Delta\alpha_{\lambda\mu}\, \delta\Delta\beta_{\alpha\beta}) + \overset{3}{C}{}^{\alpha\beta\lambda\mu}\, \Delta\beta_{\lambda\mu}\, \delta\Delta\beta_{\alpha\beta} \}\, dF , \\ \delta A_a &= \iint_F \{ p^\alpha\, \delta\overset{+}{u}_\alpha + p^3\, \delta\overset{+}{u}_3 \}\, dF + \oint_{C_t} \{ n^\alpha\, \delta\overset{+}{u}_\alpha + n^3\, \delta\overset{+}{u}_3 + m_t\, \delta\overset{+}{w}_t \}\, ds , \end{aligned} \tag{2.5}$$

valid under the constraints of the kinematic relations and of the displacement boundary conditions. In (2.5) p^i abbreviate prescribed loads on the reference surface, n^i forces and m_t tangential couples along the boundary C_t .

3. MODELLING OF REINFORCED CONCRETE

3.1 Macroscopically Uncracked Concrete

The nonlinear behavior of the concrete layers, particularly in the compression-compression-domain, is described by the **elasto-plastic-fracturing model** according to Bazant (Bazant, 1979, 1980). The advantage of this model, abbreviated in the following by EPFM, lies in a reasonably exact reproduction of typical response phenomena of concrete and in its incremental linearity. The EPFM considers concrete macroscopically as an isotropic material. Each stress increment is divided into three components:

- the elastic stress increase $\Delta\tau^{ij}_{el}$,
- the plastic stress decrease $\Delta\tau^{ij}_{pl}$,
- the stress decrease due to microcracking $\Delta\tau^{ij}_{fr}$.

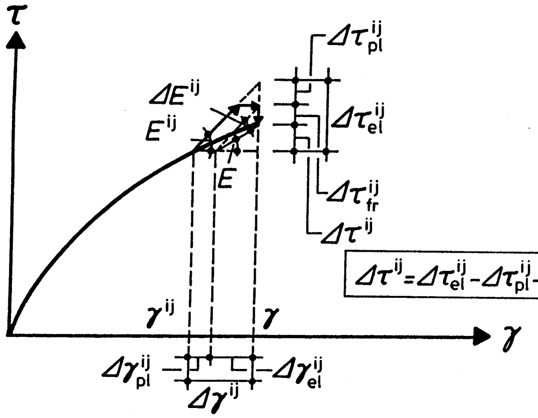

$$\Delta\tau^{ij} = \Delta\tau^{ij}_{el} - \Delta\tau^{ij}_{pl} - \Delta\tau^{ij}_{fr} \tag{3.1}$$

Fig. 2: Incremental stress decomposition of the EPFM

A **plastic yield surface** of Drucker-Prager-type describes the plastification of the concrete in the stress space and dual to this, a **fracturing surface** indicates the microcracking in the strain space. The expressions

$$\Delta\tau^{ij}_{pl} = \frac{(\frac{G}{\tau}\, s^{ij} + K\cdot\beta\cdot a^{ij})\;(\frac{G}{\tau}\, s^{km} + K\cdot\beta'\cdot a^{km})}{G + h + K\cdot\beta\cdot\beta'}\, \Delta\gamma_{km} \, , \tag{3.2}$$

$$\Delta\tau^{ij}_{fr} = \Phi \cdot (\frac{e^{ij}}{2\gamma} + \frac{\alpha}{3}\, a^{ij})\;(\frac{e^{km}}{2\gamma} + \frac{\alpha'}{3}\, a^{km})\; \Delta\gamma_{km} \; . \tag{3.3}$$

can be derived for the plastic stress decrease (pl) and the stress decrease due to microcracking (fr) by application of the above mentioned yield and fracturing conditions as well as of expanded Drucker and Iliushin stability criterions.

In (3.2, 3.3) the following abbreviations are utilized:

a^{ij} : contravariant metric tensor of the shell continuum,

s^{ij}, s_{ij} : contravariant and covariant stress deviator,

e^{ij}, e_{ij} : contravariant and covariant strain deviator,

$\tau = (\frac{1}{2} s^{ij} s_{ij})^{\frac{1}{2}}$,

$\gamma = (\frac{1}{2} e^{ij} e_{ij})^{\frac{1}{2}}$,

G, (K) : elastic shear-(bulk-) modulus,

β', (α') : internal (fracturing) friction-coefficient,

β, (α) : plastic (fracturing) dilatancy-factor,

h, (Φ) : plastic hardening (fracturing) modulus.

The material constants G, K, h, β', β, Φ, α, α' are defined by inelastic material functions of stress and strain as well as by the strength of concrete (Bazant, 1979); they were determined by empirical curve-fitting to experimental data (Bazant, 1980). Comparing the incremental constitutive law

$$\Delta\tau^{ij} = C^{ijkm}\,\Delta\gamma_{km} \tag{3.4}$$

with (3.1), the material tensor C^{ijkm} can be decomposed as

$$C^{ijkm} = C^{ijkm}_{el} - C^{ijkm}_{pl} - C^{ijkm}_{fr} , \tag{3.5}$$

with the elastic (el), plastic (pl) as well as fracturing (fr) material tensors:

$$C^{ijkm}_{el} = G\,(a^{ik}\,a^{jm} + a^{im}\,a^{jk}) + (K - \frac{2}{3}G)\,a^{ij}\,a^{km} , \tag{3.6}$$

$$C^{ijkm}_{pl} = \frac{1}{G+h+K\cdot\beta\cdot\beta'}\,(\frac{G}{\tau}\,s^{ij} + K\cdot\beta\cdot a^{ij})\,(\frac{G}{\tau}\,s^{km} + K\cdot\beta'\cdot a^{km}) , \tag{3.7}$$

$$C^{ijkm}_{fr} = \Phi\cdot(\frac{e^{ij}}{2\gamma} + \frac{\alpha}{3}\,a^{ij})\,(\frac{e^{km}}{2\gamma} + \frac{\alpha'}{3}\,a^{km}) . \tag{3.8}$$

According to (3.7, 3.8) the inelastic parts of the material tensor depend on the current states of stress and strain as well as on the load history: During the numerical evaluation they have to be updated for each change of stress and strain.

The EPFM was originally formulated for stress states in the compression-compression-domain (I in Fig. 3) only, where its high accuracy has been proved by

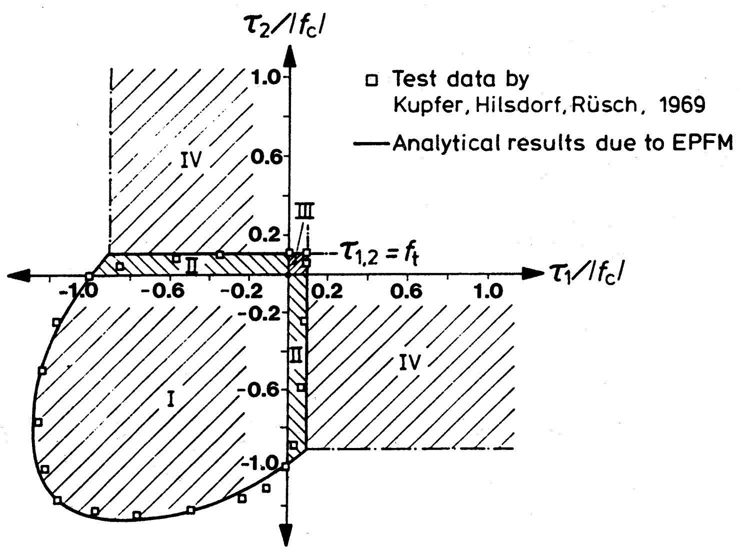

Fig. 3: Biaxial failure envelope of concrete in principal stress directions τ_1, τ_2

comparison with available experimental data. In the present work the EPFM is empirically expanded into the compression-tension-domains II and to the tension-tension-domain III, justified by the fact that plastification and microcracking occur similarly. In case of positive hydrostatic pressure the internal friction has very little influence on the plastification and is therefore neglected.

2.2 Tension Cracking of Concrete

To determine the beginning of cracking, a **principal tensile stress criterion** is applied as follows: If the tensile strength f_t of concrete is exceeded, a crack develops perpendicularly to the principal stress, whereupon the components of the material tensor in the principal stress direction are deleted. A residual shear stiffness due to aggregate interlocking is maintained, however. The resulting stress state is assumed to be uniaxial, e.g.

$$\tau^{11} = \tau^{12} = \tau^{21} = 0 \ , \qquad \Delta\tau^{11} = \Delta\tau^{12} = \Delta\tau^{21} = 0 \ :$$
$$\Delta\tau^{11} = C^{11\alpha\beta}\,\Delta\gamma_{\alpha\beta} = 0 \ , \quad \Delta\tau^{12} = \Delta\tau^{21} = C^{12\alpha\beta}\,\Delta\gamma_{\alpha\beta} = 0 \ , \qquad (3.9)$$

which yields the strain increments $\Delta\gamma_{11}$, $\Delta\gamma_{12}$ in terms of $\Delta\gamma_{22}$.

With one primary crack open, a **secondary crack** may develop perpendicularly to the first one. In this case the material tensor, with exception of its shear components $C^{1212} = C^{2112} = C^{2121} = C^{1221}$, and the complete stress tensor are equated to zero. The **re-closing** of open cracks is initiated by the following **kinematic criterion**: A crack is supposed to re-close when the corresponding strain γ^* becomes less than the cracking strain γ_c :

$$\gamma^* < \gamma_c = \gamma - f_t/E \ . \qquad (3.10)$$

After the closing of a crack, the concrete may again sustain compressive stresses, but has irreversibly lost its tensile strength in the formerly cracked direction. Other directions, however, still possess resistance to tensile stresses. To model this behavior, each layer is divided into 16 sectors. After cracking, the tensile strength in the corresponding and in both neighboring sectors is reduced to a very low value ($\approx f_t/100$).

3.3 Reinforcement

The individual bars of the reinforcement are considered as smeared into steel layers with uniaxial material properties. An elasto-plastic law with kinematic hardening and a suitable loading/unloading criterion due to Fig. 4 is applied to model the nonlinear behavior of the reinforcement.

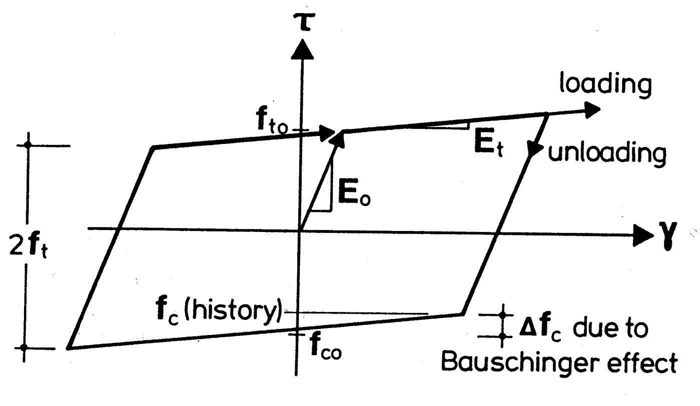

Fig. 4: Stress-strain diagram for reinforcement

3.4 Tension Stiffening

Tension stiffening is attributed to the reinforcement according to (Gilbert/ Warner, 1978). For cyclic loading the fictitious modulus of elasticity is restricted not to surpass the minimum value reached at previous states of stress.

4. FINITE ELEMENT TRANSFORMATION

4.1 Tangential Stiffness Equation

By application of a standard displacement discretization process to the kinematic fields of section 1

$$\begin{aligned} &\mathbf{u}^p = \{u_i \; w_\alpha\} , \quad \overset{+}{\mathbf{u}}{}^p = \{\overset{+}{u}_i \; \overset{+}{w}_\alpha\} , \quad \boldsymbol{\varepsilon}^p = \{\alpha_{\alpha\beta} \; \beta_{\alpha\beta}\} , \quad \overset{+}{\boldsymbol{\varepsilon}}{}^p = \{\overset{+}{\alpha}_{\alpha\beta} \; \overset{+}{\beta}_{\alpha\beta}\} : \\ &\mathbf{u}^p = \boldsymbol{\Omega}^p \, \mathbf{v}^p , \quad \overset{+}{\mathbf{u}}{}^p = \boldsymbol{\Omega}^p \, \overset{+}{\mathbf{v}}{}^p , \quad \boldsymbol{\varepsilon}^p = \mathbf{H}^p \, \mathbf{v}^p , \quad \overset{+}{\boldsymbol{\varepsilon}}{}^p = \mathbf{H}^p \, \overset{+}{\mathbf{v}}{}^p \end{aligned} \tag{4.1}$$

with $\mathbf{v}^p$ as vector of element dofs, the explained reinforced concrete shell model will be implemented into a finite element formulation. All future investigations of the present paper will be based on the **NACS48 element** (Harte/Eckstein, 1986), a 4-node shell element with 12 dofs per node for arbitrarily curved middle surfaces, using bi-cubic shape functions. Combining (4.1) and the reinforced concrete model of section 3 in (2.5), a series of lengthy transformations (Krätzig, in print) results, after assembling all finite elements of the structure, into the **global tangential stiffness equation**

$$(\mathbf{K}_{phy} + \mathbf{K}_{ge}) \cdot \overset{+}{\mathbf{V}} = \mathbf{K}_T \cdot \overset{+}{\mathbf{V}} = \mathbf{P} - \mathbf{F}_i \tag{4.2}$$

with the following abbreviations:

- $\overset{+}{\mathbf{V}}$: vector of global nodal displacement increments,
- $\mathbf{P}$: vector of global nodal loads (total),
- $\mathbf{F}_i$: vector of global internal nodal forces (total),
- $\mathbf{K}_{phy}$: elastically and physically nonlinear stiffness matrix,
- $\mathbf{K}_{ge}$: geometrical stiffness matrix.

(4.2) differs from a physically linear problem in the stiffness matrix $\mathbf{K}_{phy}$: For linear elastic responses, $\mathbf{K}_{phy}$ is constant and symmetrical. In the case of physically nonlinear material, $\mathbf{K}_{phy}$ generally is a functional of the states of stress and strain and may lose its symmetry.

4.2 Drift-Off-Reduction of Path-Tracing Algorithm

To trace arbitrary load-deformation paths by virtue of (4.2), incremental-iterative techniques, i.g. the Riks-Wempner-Wessels one (Riks, 1972, 1979; Wempner, 1971; Wessels, 1977), are applied. For materially nonlinear problems special care is required to minimize the step-size-dependence of the solution. In order to avoid accuracy manipulations on the element level each strain increment will be divided into a number of subincrements and the initial value problem solved at each material point with required acuuracy. Fig. 5 demonstrates the number of substeps with respect to a minimization of the drift-off-error from the true solution for a typical response.

Since computing time increases with the number of substeps attemps have been made to automatically determine the neccessary number of substeps: A variable C_s similar to Bergan's current stiffness parameter (Bergan/Horrigmore, 1978) is defined by

$$C_s = \frac{\det C^{\alpha\beta\lambda\rho}}{\det C_o^{\alpha\beta\lambda\rho}} , \tag{4.3}$$

characterizing the degree of nonlinearity of the current material tensor. The variable number of neccessary substeps is then determined by

$$n = n(C_s) = \Delta\gamma / \Delta\gamma_{ref} \tag{4.4}$$

with $\Delta\gamma$: actual strain increment and $\Delta\gamma_{ref}$: reference increment, empirically evaluated by numerical experiments. Results of the above mentioned scheme are presented in Fig. 5: The total number of substeps dropped from 380 (10 substeps for each iteration) to 112 without significant loss of accuracy (Zahlten, in print).

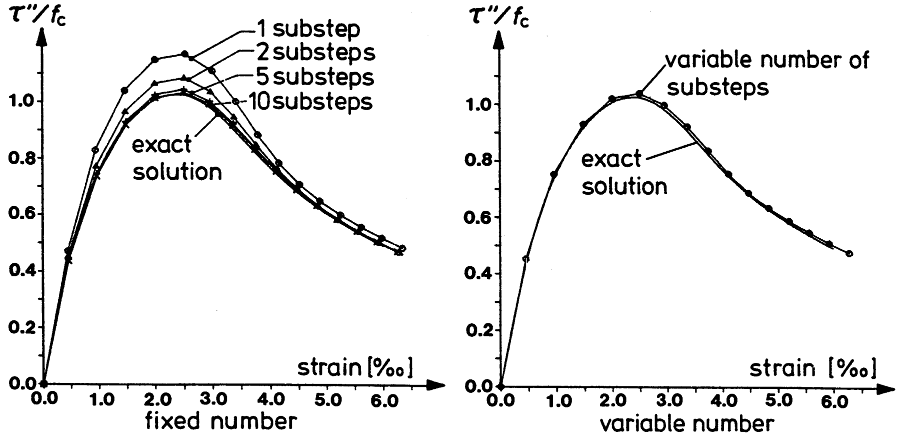

Fig. 5: Influence of number of substeps on accuracy of solution

5. NUMERICAL STUDIES

5.1 Simply Supported Square Plate

Fig. 6 illustrates geometry, material properties and reinforcement of a simply supported slab. This structure was tested under uniform transverse load p up to collapse by (Taylor/Maher/Hayes, 1966) and recently analyzed by (Arnesen, 1979) and (Van Greunen, 1979). It is reported that geometrical nonlinearities besides physical ones strongly influence the load bearing capacity of this structure leading to significantly higher, i.e. more realistic collapse loads.

In our analysis one quarter of the plate is discretized into 3x3 NACS48 elements. Fig. 7 demonstrates the centerpoint deflection plotted against the load intensity. Obviously, the present analysis exhibits a too soft response after the occurence of the first cracks, probably because of unfavorably low tensile strength and tension stiffening assumed. At higher load levels, however, the deviation from the test response becomes smaller with an excellent approximation of the failure load (failure criterion: $\Delta p = 0$).

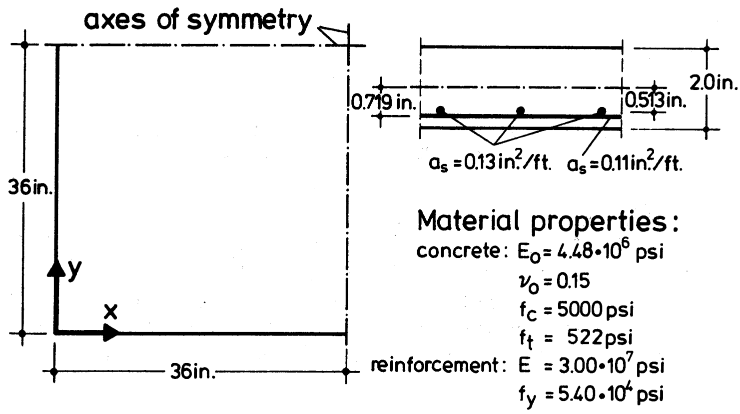

Fig. 6: Simply supported square slab under transverse pressure p

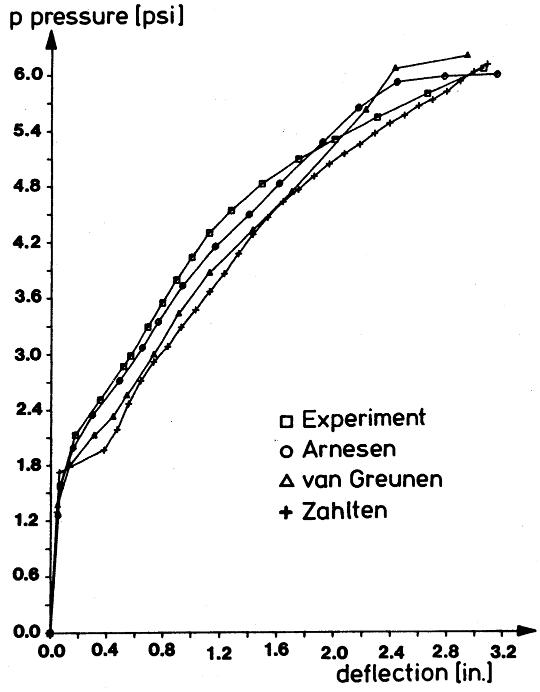

Fig. 7: Geometrically and physically nonlinear response, centerpoint deflection

5.2 Collapse Analysis of Natural Draught Cooling Tower

The next example presents the collapse analysis of a natural draught cooling tower under dead load g and quasi-static wind load w (Krätzig/Zhuang, in print). The tower has 159.15 m of height, 89.20 m upper and 128.80 m base diameter. The wall thickness reduces near the throat from its standard value 0.22 m to 0.16 m. Sufficiently rigid ring-beams stiffen both edges of the shell. The concrete is assumed to have a compressive (tensile) strength of 33.894 MN/m² (3.890 MN/m²).

The analysis uses 8 NACS48 elements for half the circumference and 12 in meridional direction. Moreover 8 layers were combined over the thickness to model the reinforced concrete shell. A Newton-Raphson scheme was applied to solve (4.2) in an incremental-iterative sense.

The collapse analysis was performed for the limit state

$$p = 1.3\ g + 1.5\ g \qquad (5.1)$$

according to the CEB-Model Code. The resulting load p, multiplied by a factor λ, has been increased until failure. Fig. 8 depicts the load-displacement path of the normal displacement v_3 of the shell at $\Theta^1=67°$ and $z=145.65$ m,

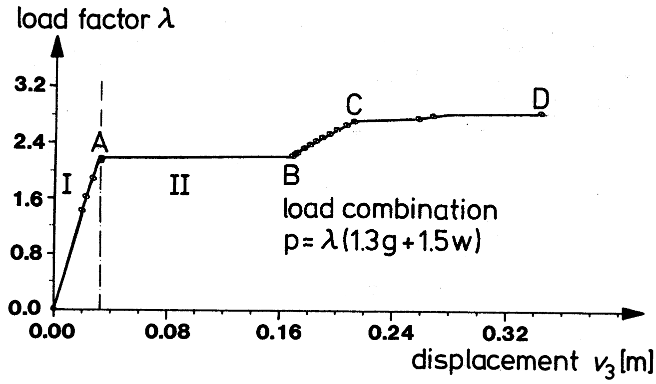

Fig. 8: Geometrically and physically nonlinear response, load-deflection curve at $\Theta = 67°$, $z = 145.65$ m

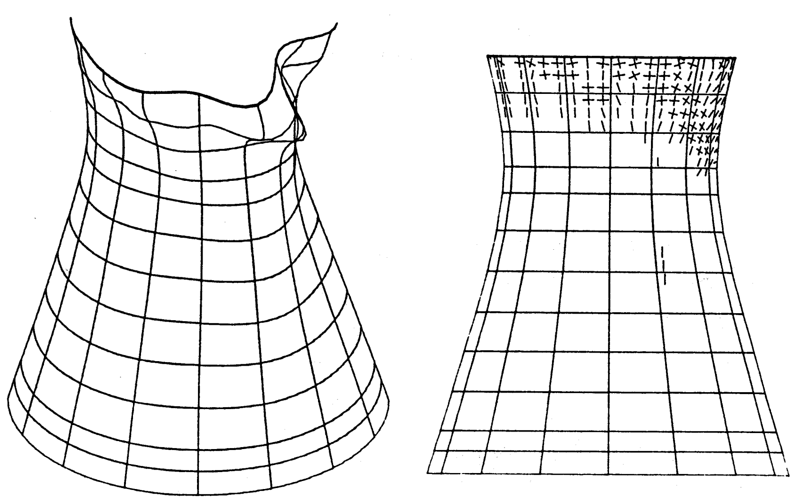

Fig. 9: Deformation pattern and smeared cracks on the outer face before failure

the position of the maximum bulge (Fig. 9). In domain I in Fig. 8 the cooling tower shell responds crack-free owing to the tensile strength of the concrete. At point A the first cracks occur in meridional direction near the upper rim.

Between A and B, cracking spreads over the upper part of the shell down to the waist causing large displacements. From point B to C the tensile stresses, originally carried by the concrete, are rearranged to the circumferential reinforcement in the cracked zones. At point C yielding occurs, leading to rapid secondary cracking in the upper parts with increased deformations and local bulges. Finally the reinforcement there enters a state of full plastification and the structure becomes unstable (point D).

5.3 Impact Analysis of a Simply Supported Beam

In the late seventies the BAM in Berlin has tested a series of simply supported beams under impact loading. One of them, beam No. 115 (Fig. 10), has been selected to demonstrate the capability of the presented finite element concept to model also dynamic processes. The test beam failed after 59 ms by rupture of the lower reinforcement with a deflection of 21,6 cm. Our received results are compared with the experimental data and with numerical studies by (Emrich/Herter/Puffer, 1982) and (Steberl, 1986).

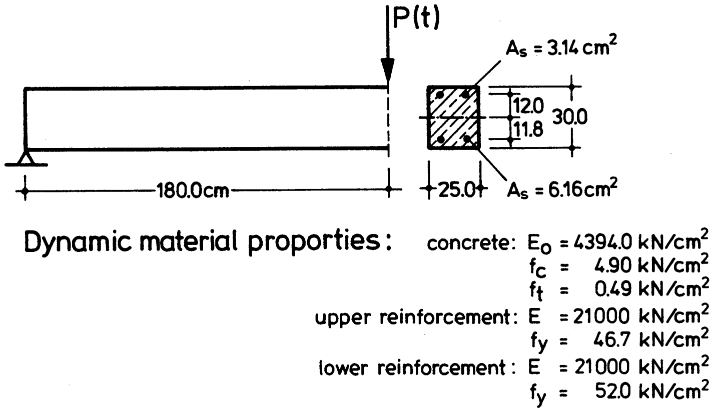

Fig. 10: Simply supported beam under impact load

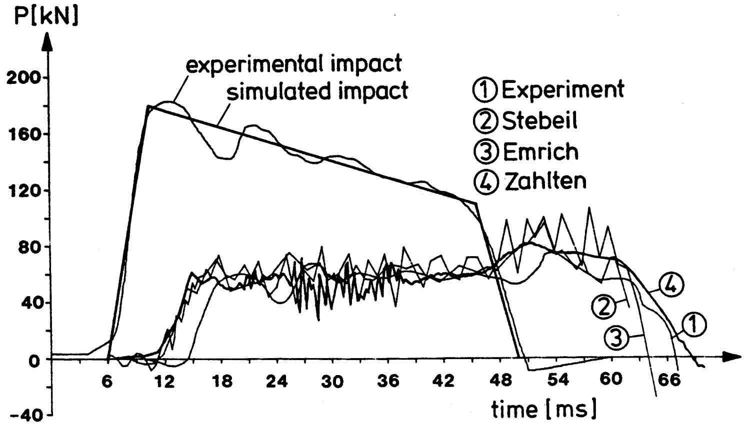

Fig. 11: Time-histories of impact and reaction forces

To include strain-rate effects into the material parameters, an increase of 20% for the concrete strength f_c and 10% for the yield stress f_y of the reinforcement are assumed. A Newmark-algorithm with Newton-Raphson-iterations has been selected for the integration of the tangential equation of motion (Krätzig, in print; Zahlten, in print), in which a Raleigh-damping of 2% was introduced. The experimental impact and reaction forces as well as numerically evaluated time-histories are compared in Fig. 11, the midspan deflections in Fig. 12, all with satisfactory agreement.

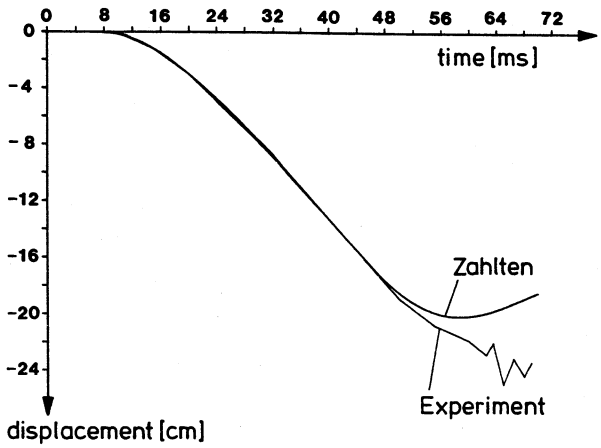

Fig. 12: Time-history of midspan deflections

6. CONCLUSIONS

The paper demonstrates the efficiency of a layered model for reinforced concrete shells on the basis of the plastic-fracturing theory by Bazant. It emphasizes the general advantage of an incrementally linear concept and stresses its numerical stability by example of several computed responses.

ACKNOWLEDGEMENT

Parts of the paper were prepared within projects of the Research Center for Structural Dynamics - SFB 151 at the Ruhr-University and within the DFG - Research Program on Nonlinear Computational Mechanics. Financial support of the German Science Foundation - DFG is gratefully acknowledged.

REFERENCES

Basar, Y., Krätzig, W.B. (1985). Mechanik der Flächentragwerke. Verlag Friedr. Vieweg & Sohn, Braunschweig/Wiesbaden.

Basar, Y. (1986). Zur Struktur konsistenter inkrementeller Theorien für geometrisch nichtlineare Flächentragwerke und deren Operatordarstellung. Ingenieur-Archiv 56, 209-220.

Bazant, Z.P., Kim, S.-S. (1979). Plastic-Fracturing Theory for Concrete. J. Eng. Mechanics Div., Proc. ASCE, 105, 407-428.

Bazant, Z.P. (1980). Work Inequalities for Plastic Fracturing Materials. Int. J. Solids Structures, 16, 873-901.

Gilbert, R.I., Warner, R.F. (1978). Tension Stiffening in Reinforced Concrete Slabs, J. Struct. Div., Proc. ASCE, 104, 1885-1900.

Harte, R., Eckstein, U. (1986). Derivation of Geometrically Nonlinear Finite Shell Elements via Tensor-Notation. Int. J. Num. Meth. Eng. 23, 367-384.

Krätzig, W.B. (in print). Eine einheitliche statische und dynamische Stabilitätstheorie für Pfadverfolgungsalgorithmen in der numerischen Festkörpermechanik, ZAMM.
Riks, E. (1972). The Application of Newton's Method to the Problem of Elastic Stability. J. Appl. Mech. 39, 1060-1066.
Riks, E. (1979). An Incremental Approach to the Solution of Snapping and Buckling Problems. Int. J. Solids Struct. 15, 529-551.
Wempner, G.A. (1971). Discrete Approximations Related to Nonlinear Theories of Solids, Int. J. Solids Struct. 7, 1581-1599.
Wessels, M. (1977). Das statische und dynamische Durchschlagsproblem der imperfekten flachen Kugelschale. Mitt. d. Inst. f. Statik Nr. 23, T.U. Hannover.
Bergan, P.G., Horrigmoe, G., Krakeland, B., Soreide, T.H. (1978). Solution Techniques for Nonlinear Finite Element Problems. Int. J. Num. Meth. Eng., 1677-1696.
Zahlten, W. (in print). Ein Beitrag zur physikalisch und geometrisch nichtlinearen Computeranalyse allgemeiner Stahlbetonschalen, Bochum.
Taylor, R., Maher, D.R.H., Hayes, B. (1966). Effect of the Arrangement of Reinforcement on the Behavior of Reinforced Concrete Slabs. Magazine of Concrete Research, Vol. 98, No. 55.
Arnesen, A. (1979). Analysis of Reinforced Concrete Shells Considering Material and Geometric Nonlinearities. Norwegian Inst. of Techn., Univ. of Trondheim, Div. of Struct. Mech., Report No. 79-1.
Van Greunen, J. (1979). Nonlinear Geometric, Material and Time Dependent Analysis of Reinforced and Prestressed Concrete Slabs and Panels. University of California, Berkeley, Div. SESM, Report No. 79-3.
Krätzig, W.B., Zhuang, Y. (1989). Nonlinear Physical and Geometrical Collapse Analysis of Cooling Towers. Proc. 3. Int. Conf. on Nat. Draught Cooling Towers, Paris.
Emrich, F., Herter, J., Puffer, G. (1982). Nonlinear Finite Element Analysis of Reinforced Concrete Beams under Impact Load in Comparison with Experimental Results. Proc. Symp.: Concrete Struct. under Impact and Impulsive Loading, BAM, Berlin.
Steberl, R. (1986). Berechnung stoßartig beanspruchter Stahlbetonbauteile mit endochronen Werkstoffgesetzen. Berichte aus dem Konstruktiven Ingenieurbau, Heft 6, Werner-Verlag, Düsseldorf.